



## Advanced acoustic measurement system for rocket noise source characterization<sup>i</sup>

Michael M. James<sup>a)</sup>

Blue Ridge Research and Consulting, LLC  
15 W. Walnut St., Suite C, Asheville, NC 28801

Kent L. Gee<sup>b)</sup>

Department of Physics and Astronomy  
Brigham Young University, N243 ESC, Provo, UT 84602

**Development of the next generation of space flight vehicles has prompted a renewed focus on sound source characterization and near-field propagation modeling. Without advancements in these areas, large uncertainties in vibroacoustic loading estimates on space vehicles and payloads may result in structural designs that are either insufficient or excessive. Improved measurements in an extreme environment are essential to the characterization of rocket aeroacoustic source properties, which in turn provide inputs to empirical models, allow validation of computational models, and, ultimately, lead to optimal structural designs. As part of this effort, an advanced acoustical measurement, analysis, and data visualization system is being developed. An overview of the system design and initial measurements on an Orion 50S XLG solid rocket motor are described.**

### 1 INTRODUCTION

Accurate estimates of the vibroacoustic loading on space vehicles and payloads during launch require knowledge of the rocket noise source properties and near-field acoustic energy flow characteristics. Measurements of the noise near the rocket plume are critical, not only to directly determine the noise environment, but also to provide inputs to empirical models and to validate computational aeroacoustics models. However, these measurements are difficult to obtain because of the extreme nature of the acoustic and temperature environments, especially in the near field. These challenges have generally resulted in the use of far-field measurement data<sup>1,2,3,4,5</sup> to infer acoustic source properties such as near-field directivity and total radiated power. However, these far-field measurements are difficult to interpret, first because of the

---

i) SBIR Data Rights (see §6)

a) email: michael.james@blueridgeresearch.com

b) email: kentgee@byu.edu

difficulty in defining the far field, and second, because of terrain, meteorological, and angle-dependent nonlinear effects.

In the near field, even well-made acoustic pressure measurements are insufficient. A set of pressure measurements can reveal the local sound pressure levels at the sensor locations. However, because of the frequencies and source size inherent to a rocket plume, it would require an extremely large array of distributed microphones to adequately map out the critical near-field region and establish how the sound energy is traveling outside that region. Because of that deficiency, NASA has sought solutions to better understand the near-field acoustic energy flow. An improved system for determining this near-field energy flow provides source characterization capabilities beyond traditional pressure measurements. Blue Ridge Research and Consulting, LLC (BRRC), in collaboration with Brigham Young University (BYU), has explored innovations to expand and improve the concept of acoustic energy-based (e.g., intensity) measurements and analysis in the near-field of rocket plumes.

## **2 MEASUREMENT SYSTEM DESIGN**

Acoustic measurements of the rocket plume are critical to providing a better understanding of the rocket source region; however, these measurements are difficult to conduct because of the extreme nature of the acoustic and temperature environments near the rocket plume and the large size of the rocket noise source. With these constraints in mind, an energy-based measurement probe and analysis method is being developed to measure the magnitude, directivity, and spectral content of the rocket source.<sup>6,7</sup> Determination of these quantities over a sufficiently large spatial aperture near the rocket should provide insight into physical noise generation mechanisms in the turbulent flow field.

The application of energy-based processing to the characterization of a full-scale rocket plume and the development of an appropriate measurement system poses several technical and logistical challenges. Accurate characterization of the acoustic pressures in the near field of a high-thrust rocket requires the ability to record peak sound pressure levels up to 180 dB and frequencies from 5 Hz to 40 kHz. In addition, measurements must be made along the entire length of the plume, which can extend up to 100 m or longer. The measurement system must be semi-portable because of the limited set of locations where rockets can perform static firings, and its components, from the microphones to the data recorder, must be rugged so that it can withstand the vibration and temperature loading during rocket tests. Finally, the system must integrate the technical requirements for energy-based measurements with the environmental conditions and the safety constraints involved with rocket noise measurements. The design of each of the system components is described below.

### **2.1 Energy-based Acoustic Probe**

A multi-axis energy-based probe suitable for rocket noise measurements consists of multiple well-matched, low-sensitivity microphones that can be used to calculate collocated particle velocity and pressure estimates required in quantities such as active and reactive intensity, and kinetic, potential, and total energy densities. Tetrahedral (three-axis) probe prototypes were developed as part of a previous effort,<sup>6</sup> referred to in Fig. 1 as the spherical and external frame probes. As part of the current investigation, a parallel-axis probe, wherein all four microphones are oriented in the same direction, is being evaluated. As shown in the figure, this probe has advantages in that no microphones need be oriented toward the plume, which has important implications in microphone power requirements to properly sense acoustic shocks.

## **2.2 Data Acquisition System**

The heart of the measurement system is a National Instruments (NI) PXI data acquisition system chosen for its flexibility, scalability, and cost effectiveness. The ability to scale the number of data channels and microphones provides the ability to increase the number of probes based on the size of the rocket, in addition to providing additional channels for supporting pressure, vibration, and temperature measurements. The PXI chassis include up to 18 dynamic signal acquisition (DSA) modules with simultaneous sampling to insure correct phasing of all channels. With 24-bit analog inputs and IEPE constant-current signal conditioning, the DSA modules are ideal for making precision measurements. The modules deliver 113 dB of dynamic range and simultaneous sampling on all channels at rates up to 204.8 kS/s. Digitized data from all channels is streamed over a single coaxial or optical cable to a high powered Intel processor based Microsoft Windows 7 controller. The controller has four solid state drives (SSD), preferred over traditional hard disk drives for their robustness, increased vibration tolerance, and superior write speed. The SSDs are deployed in a RAID 10 configuration, which is optimal for mission critical applications as the data is striped across two SSDs for increased performance and mirrored across two SSDs for redundancy in case of drive failure.

Data is acquired using custom-built NI LabVIEW based software, which provides the capability to tailor the setup, monitoring, and data verification. Setup controls provide selectable sensor type, sensitivity, gains, conditioning, calibration, and monitoring on an individual channel basis. Experimental setup is aided by real-time multiple-channel monitoring of time histories, overall and peak levels, and ANSI compliant full and fractional octave analysis. The scaled data is saved in a non-proprietary binary format. Data acquisition control and monitoring are performed using a daylight-readable laptop computer running Windows Remote Desktop. The computer can be used either wirelessly or wired to the controller.

The harsh environment generated by a rocket plume dictates special considerations in the design, layout, and operation of the data acquisition system. To increase the system's tolerance to vibration the data acquisition system is housed in a vibration-isolated rack-mounted military specification shipping container. The location of the data acquisition system in the field dictates a tradeoff between minimizing vibration and temperature loading and increased cabling and setup time. To comply with safety requirements recordings are time triggered to allow for unattended usage. Extensive component testing of the instrumentation and data acquisition software has been performed in both the laboratory and the rocket plume environment to ensure proper functioning. The acoustical instrumentation testing focused on the robustness and scalability of the system. The 24-bit data acquisition system has been successfully tested with over 100 channels simultaneously sampled at a rate of 200 kHz.

## **3 FIELD MEASUREMENTS**

### **3.1 Test Description**

Special arrangements were made by NASA Marshall Space Flight Center (MSFC) and Alliant Techsystems (ATK) to enable the BRRC/BYU team to participate in a ground-based midcourse defense (GMD) Stage 1 horizontal static test conducted at ATK's Promontory, Utah facility on 24 June 2010. This test occurred at ATK's T-6 test facility at approximately 11:06 a.m. Mountain Daylight Time (MDT). The GF058, or Orion 50S XLG, motor, has a 0.91-m (3-ft) diameter nozzle and generates an average/maximum thrust of 592/672 kN (133,193/151,098 lbf) with a burn time of 68 seconds. The motor's predicted maximum (vacuum) thrust occurs about 15 seconds after ignition and then remains fairly steady throughout

the remainder of the test. Photographs of this test were taken from the T-6 and the T-97 viewing area, approximately 1200 m away, as shown in Fig. 2.

In coordination with this event, the BRRC/BYU team conducted a measurement program designed to field test prototype designs of the three types of tetrahedral probes and the data acquisition system. The purpose of this measurement program was to evaluate the performance of these instruments during a rocket static firing.

### 3.2 Measurement Layout

On the two days prior to the static firing, measurement instrumentation was deployed in a field adjacent to the T-6 test facility, as shown in Fig. 3. Measurement location distances are described in terms of nozzle diameters ( $D$ ) with  $1D$  equaling 0.91 m; angles are with respect to the motor exhaust direction. Three linear arrays, consisting of energy-based probes, pressure microphones, accelerometers, and meteorological sensors, were deployed.

The shear-layer array, indicated by the red dotted line in Fig. 3, was offset by  $10D$ , 9.14 m, from the exhaust plume shear-layer boundary, which itself was estimated to be at a  $20^\circ$  angle to the motor centerline (including a  $5^\circ$  motor gimbal angle). This location permitted making acoustic measurements in the near-field environment while being far enough away from the plume to ensure that the instrumentation operated properly. Shear-layer measurement location distances are measured from the nozzle exit plane.

Three 2.54-cm (1-in) spherical probes were deployed in the shear-layer array at distances of  $13D$ ,  $20D$ , and  $33D$ . The  $20D$  spherical probe was part of a cluster of four different probes being tested at the  $20D$  shear-layer location; these also included a 2.54-cm parallel axis probe and two external frame probes (2.54 cm and 10.2 cm (4 in)). Note that the characteristic size of the probes is defined by the diameter of the sphere circumscribing the microphones. Fig. 4 shows the probe orientations and probe cluster geometry. Of importance for further discussion is the fact that, for the spherical probes, microphone  $B$  was oriented toward the plume. For the external frame probes, microphone  $C$  pointed toward the plume. In addition to the four types of probes, there were also pressure microphones, accelerometers, and meteorological sensors located at measurement points along the shear-layer array.

Two additional radial arrays were oriented at  $60^\circ$  and at  $90^\circ$  to the motor centerline, indicated in Fig. 3 by the blue and purple dotted lines, respectively. Distances along the radial arrays were measured from the estimated peak source location, which is  $15D$  downstream of the nozzle. Sensors deployed in the  $60^\circ$  and  $90^\circ$  radial arrays included two-dimensional 2.54-cm parallel axis probes, individual microphones, and meteorological sensors. In addition, a single 2.54-cm spherical probe was deployed on the  $75^\circ$  radial at a distance of  $33D$ .

### 3.3 Instrumentation

The measurement system was an NI PXI platform data recorder with PXI-4462 data acquisition cards (24-bit A/D conversion). Data channels were routed through an NI BNC-2144 BNC-to-InfiniBand breakout box to InfiniBand connectors which connected directly to the DSA modules. This grouping limited the number of cables and complexity of the system by running one InfiniBand cable for every eight channels. For several remote microphone locations, data channels were also connected to the recorder via separate BNC cables. Noise and vibration data were recorded on 47 channels using a sampling rate of 204.8 kHz. The data acquisition system was located in an enclosed utility room adjacent to the T-6 control room and forward of the motor test bay.

High amplitude pressure measurements were made using the 2.54-cm spherical probes with 6.5-mm ( $1/4$ -in) G.R.A.S. 40 BH externally polarized microphones and 26CB preamplifiers. This

microphone-preamplifier pairing has a frequency response of 10 Hz to 20 kHz ( $\pm 3$ dB). Identical microphones and preamplifiers were also used with the 2.54-cm external frame probe. In the 10.2-cm external frame probe and in the 3-D 2.54-cm parallel axis probe, 6.5-mm G.R.A.S. 40 BD ICP pressure microphones, with a frequency response of 10 Hz to 70 kHz, were used. Pressure measurements using individual microphones were also conducted at various other locations using 3.2-mm ( $\frac{1}{8}$ -in) 40 DD pressure microphones, with an extended frequency response of 6.5 Hz – 140 kHz, and 6.5-mm 40 BD pressure microphones. A calibration check was done before and after the test using a GRAS 114 dB acoustic calibrator.

## 4 RESULTS

### 4.1 Overall and Spectral Levels

Maps of overall sound pressure level (OASPL) and peak sound pressure level across the measurement positions in Fig. 3 are displayed in Fig. 5. All measurement locations are shown with respect to the rocket motor exit plane, located at the plot origin, with the exhaust direction aligned with the positive vertical axis. Although the array is sparse beyond a sideline distance of  $33D$ , the density of the sensor array closer in shows the directionality and the downstream location of the maximum overall levels. The peak levels show a crest factor of 15-20 dB, with peak levels exceeding 175 dB (peak pressures of 11 kPa) at the closest measurement locations.

The power spectral density (PSD) and the one-third octave band spectral map of the shear-layer array are shown in Fig. 6. The choice of  $15D$  as the origin was not inappropriate, but note also the extent of the dominant overall region in the shear layer; the 3-dB-down range extends approximately  $33D$ . Also of interest is the low frequency PSD of the  $10D$ ,  $13D$ , and  $20D$  measurements nearest to the nozzle exit; these exhibit almost no decay over the 10-Hz to 100-Hz frequency range. Further investigation is warranted. The spectral map clearly shows a dominance of higher frequency energy closer to the nozzle exit with a spectral shift to lower frequency for measurements down the plume.

The PSD along the  $60^\circ$  and  $90^\circ$  radial microphone arrays are shown in Fig. 7. The spectral slope of  $f^2$  at low frequency and  $1/f^2$  at high frequency, indicated by the straight dashed lines, are very close to those expected for sawtooth waves and to those measured for  $N$  waves.<sup>8,9</sup> The  $1/f^2$  drop-off in the PSD indicates the high-frequency end of the spectrum is controlled by shocks,<sup>10</sup> even at  $133D$ , with no evidence at high frequencies of a more rapid drop-off due to atmospheric absorption. The peak frequency along the  $60^\circ$  radial microphone array shifts progressively lower at greater distance, from 100 Hz at  $23D$  to 50 Hz at  $133D$ . This spectral shift in peak frequency indicates the strong influence of the low frequency energy generated farther downstream. Also note that as the distance increases along the radial, evidence of ground absorption in the higher frequency spectra becomes more prevalent. The peak frequency along the  $90^\circ$  radial microphone array is nominally 100 Hz, with the exception of the  $15D$  measurement location, which exhibits a strong dip in the spectra at 100 Hz, believed to be a result of ground interference.

In addition to acoustic field characterization, acceleration measurements were performed to determine the vibration loading on the microphones and data acquisition system. The sensitivity of a microphone to vibration normal to the diaphragm is well defined as it is determined by the mass of the diaphragm, and for  $1 \text{ m/s}^2$  is of the order of 65 dB (SPL)<sup>11</sup>. The sensitivity to vibration is much smaller in all other directions. To study this effect a microphone located on the  $60^\circ$  radial array  $33D$  from the estimated source was chosen. This pressure microphone was oriented vertically for grazing incidence. An accelerometer was positioned directly under the microphone, also in a vertical orientation. The power spectral density and overall levels of the microphone and accelerometer are shown in Fig. 8. The figure clearly demonstrates that the

acceleration spectrum did not impact the pressure spectrum at any frequency. (Note the pressure and acceleration power spectral density data, while displayed on the same plot, cannot be directly compared in terms of level). The measured levels at the data acquisition system located in the T-6 pump room were found to be insignificant, on the order of  $0.1 G_{\text{rms}}$  and  $0.5 G_{\text{peak}}$ . The levels near the plume were much more significant with the accelerometer located  $27D$  along the  $20^\circ$  shear layer array, reaching levels of  $14 G_{\text{rms}}$  and  $248 G_{\text{peak}}$ .

Temperatures were also recorded at all measurement locations except for the most distant locations in the 60-degree and 90-degree arrays. A spatial color map of the peak recorded temperatures is shown in Fig. 8. In examining the temperature time histories, it is apparent that the recorded temperatures peaked at the end of the static firing. Therefore, actual maximum temperatures were not recorded during the test due to insufficient response time of the probes. Peak temperatures recorded across the array indicates that a negative temperature gradient of approximately  $70^\circ\text{F}$  existed between the downstream position at  $10D$  and  $13D$ , closest to the nozzle, and the downstream position at  $33D$ . It also appears from the time histories that the rate of increase in temperature is progressively smaller along the array in the downstream direction. Both of these gradients, for temperature and temperature rate, need to be further defined in order to better characterize the near-field rocket plume environment and to understand how these mechanisms effect nonlinear sound propagation.

## 4.2 Vector Probe Analysis

The objective of the data acquisition is to produce maps of energy quantities near the rocket motor. However, the calculation of any derived quantity is only as good as the pressure measurement. The power spectral densities for the four probes located in the cluster are displayed in Fig. 9. The four individual microphone measurements on each probe are very similar except at high, and sometimes low, frequencies. The high-frequency variation is caused by diffraction/scattering around the different microphones. The spherical probe results in a more systematic, although greater, scattering. The parallel axis probe scattering starts at a few kHz, but the overall variation is less than that of the external frame probes. Note that the scattering is less for the external frame probe with the larger separation distance. The worst diffraction (excess high-frequency response) occurs for microphone *B* with the spherical probe and microphones *C* for the external frame probes because they are pointed toward the plume, a nonideal orientation for a pressure microphone.

The high-frequency artifacts induced by nonideal orientation have another consequence. Because the high frequencies are associated with acoustic shocks, their incidence on a microphone cause a rapid voltage change with respect to time, requiring sufficient instantaneous power handling capability by the microphone power supply (whether constant voltage or constant current). When this is the case, there is a capacitive discharge effect present in the waveform, resulting in increased levels at low frequencies,<sup>12,13</sup> as seen in Fig. 9. This effect occurs most predominantly for a given probe at the microphones nominally facing the plume. Because of these issues, the parallel axis probe, wherein the microphones can all be aligned for essentially grazing incidence, appears to be a good compromise in terms of probe design.

The most immediately useful energy-based quantity is active vector intensity. The horizontal intensity has been calculated for all nine probes. This is displayed in Fig. 10 for various frequencies. At 50 Hz, the small spacing for most of the probes results in meaningless intensity vectors. The three exceptions are the 10.2-cm external probe located in the shear-layer cluster and the two-dimensional parallel axis probes located along the two radials. The greater spacing allows for more accurate estimation at these lower frequencies where the acoustic phase difference is relatively small. At 150 Hz, where all of the probes are within their operational

bandwidths, the intensity vectors, which are scaled by the cube root of the magnitude, show that the dominant intensity is  $33D$  downstream. As frequency increases, the directivity shifts more toward the sideline, and the maximum source region appears to contract slightly and move upstream. The contraction of the source region can be seen by the reduction in the radial probe intensity vectors relative to those of the shear layer, signifying more spherical spreading. By 3 kHz, however, the maximum bandwidth of the probes with greater microphone spacing has been exceeded, using the traditional finite-difference/sum-based intensity processing technique. High-frequency improvements should be achievable using the wave-vector method<sup>14</sup> developed at BYU.

### **4.3 Lessons Learned**

Data collected in the Orion-50 measurement provides valuable information needed to refine and improve the measurement system. The spherical probe prototype, developed during a previous effort, relied on four microphones requiring a 200-V polarization voltage (and a separate power supply), arranged in tetrahedral fashion, and flush mounted in an aluminum sphere. Design changes investigated in the current study consist of the use of low-sensitivity pre-polarized microphones to eliminate the requirement for a separate power supply, alternative microphone orientations and spacing, and the use of a mounting scheme that permits microphones and preamplifiers to be removed and calibrated in place of the permanent mounting required by the spherical housing. Results show that pre-polarized microphones held in a tetrahedral arrangement promise comparable performance to, but greater flexibility and long-term robustness than, the spherical probe.

The observed saturation issues, which consist of a capacitive discharge and a subsequent resettling of the data in both pre-polarized and traditionally powered microphones, are most significant on the channels corresponding to the microphones pointing toward the plume, a nonideal orientation for a pressure microphone. This suggests that the parallel axis probe, wherein none of the microphones point toward the plume, has significant advantages. The intensity plots demonstrate the advantage of the greater microphone spacing achieved with the 10.2-cm external frame probes over the 2.54-cm probes in resolving low frequency intensity quantities, which can be significant for full-scale rocket motors.

## **5 CONCLUDING DISCUSSION**

Intensity-based quantities can provide important information about rocket plume source characteristics that traditional scalar acoustic pressure alone cannot. A small experimental array of energy-based measurement probes successfully characterized the acoustic source size, frequency content, and directivity of the Orion-50 50S XLG plume. To achieve a similar amount of detail using traditional approaches would require an extremely large array of distributed microphones to adequately map the near-field region and establish how the sound energy is traveling outside that region. The development of a rocket noise source measurement protocol based on the combination of an array of probes and scalar sensors will result in a less complex, and more robust, approach to source characterization than can be achieved with traditional methods. The proposed approach provides both near-field source characteristics and the ability to infer far-field directivity. Future efforts will focus on investigation of the use of additional energy-based quantities to gain further insight into the near-field acoustic environment.

## **6 ACKNOWLEDGEMENTS**

The authors wish to thank Dr. Jeremy Kenny of NASA Marshall Space Flight Center and Dr. William W. St. Cyr of NASA Stennis Space Center and for supporting the Blue Ridge

Research and Consulting (BRRC) and Brigham Young University (BYU) team. We also extend our gratitude to ATK Test Services and especially to Sharon Dressen, Kevin Rees, Roy Norris, and the T-6 test facility personnel who helped to make this a successful effort.

*SBIR Data Rights<sup>i)</sup> - These SBIR data are furnished with SBIR rights under Contract No. NNX11CC16C. For a period of 4 years, unless extended in accordance with FAR 27.409(h), after acceptance of all items to be delivered under this contract, the Government will use these data for Government purposes only, and they shall not be disclosed outside the Government (including disclosure for procurement purposes) during such period without permission of the Contractor, except that, subject to the foregoing use and disclosure prohibitions, these data may be disclosed for use by support Contractors. After the protection period, the Government has a paid-up license to use, and to authorize others to use on its behalf, these data for Government purposes, but is relieved of all disclosure prohibitions and assumes no liability for unauthorized use of these data by third parties. This notice shall be affixed to any reproductions of these data, in whole or in part.*

## 7 REFERENCES

1. K. M. Eldred, "Acoustic Loads Generated by the Propulsion System," NASA SP-8072, June 1971.
2. Cole, J. N., von Gierke, H. E., Kyrakis, D. T., Eldred, K. M., and Humphrey, A. J., "Noise Radiation from Fourteen Types of Rockets in the 1,000 to 130,000 Pounds Thrust Range," Wright Air Development Center (WADC) Technical Report 57-354, December 1957.
3. R. J. Kenny, C. Hobbs, K. Plotkin, and D. Pilkey, "Measurement and Characterization of Space Shuttle Solid Rocket Motor Plume Acoustics," AIAA paper 2009-3161, May 2009.
4. J. Haynes, and R. J. Kenny, "Modifications to the NASA SP-8072 Distributed Source Method II for Ares Lift-off Environment Predictions," AIAA paper 2009-3160, May 2009.
5. K. J. Plotkin, L. C. Sutherland, and B. T. Vu, "Lift-off Acoustics Predictions for the Ares I Launch Pad," AIAA paper 2009-3163, May 2009.
6. K. L. Gee, J. H. Giraud, J. D. Blotter and S. D. Sommerfeldt, "Energy-based acoustical measurements of rocket noise," AIAA paper AIAA 2009-3165, May 2009.
7. K. L. Gee, J. H. Giraud, J. D. Blotter, and S. D. Sommerfeldt, "Near-field acoustic intensity measurements of a small solid rocket motor," J. Acoust. Soc. Am. 128, EL69-EL74 (2010).
8. B. Lipkens, "Model experiment to study sonic boom propagation through turbulence. III. Validation of sonic boom propagation models," J. Acoust. Soc. Am. 111, 509-519 (2002).
9. S. A. McInerny, S. M. Olcmen, "High-intensity rocket noise: Nonlinear propagation, atmospheric, absorption, and characterization," J. Acoust. Soc. Am. 117 (2), 578-591 (2005).
10. Nonlinear Acoustics, edited by M. F. Hamilton and D. T. Blackstock (Academic, San Diego, 1998).
11. Bruel & Kjaer Microphone Handbook, Vol. 1: Theory, BE 1447-11.
12. R. T. Taylor, K. L. Gee, J. H. Giraud, S. D. Sommerfeldt, J. D. Blotter, and C. P. Wiederhold, "On the use of prepolarized microphones in rocket noise measurements," J. Acoust. Soc. Am. 130, 2512 (2011).
13. R. T. Taylor, "Microphone system response in high amplitude noise environments," Senior Thesis, Dept. of Physics and Astronomy, Brigham Young University, Aug. 2011.
14. D. C. Thomas, "Theory and estimation of acoustic intensity and energy density," M.S. Thesis, Dept. of Physics and Astronomy, Brigham Young University, Aug. 2008.



*Fig. 1 – Microphone configurations evaluated in the study. Left: spherical probe, center: external frame probe, right: parallel axis probes.*



*Fig. 2 - GMD stage 1 Orion-50 horizontal static firing observed from above the test cell (left) and from the T-97 viewing area (right).*

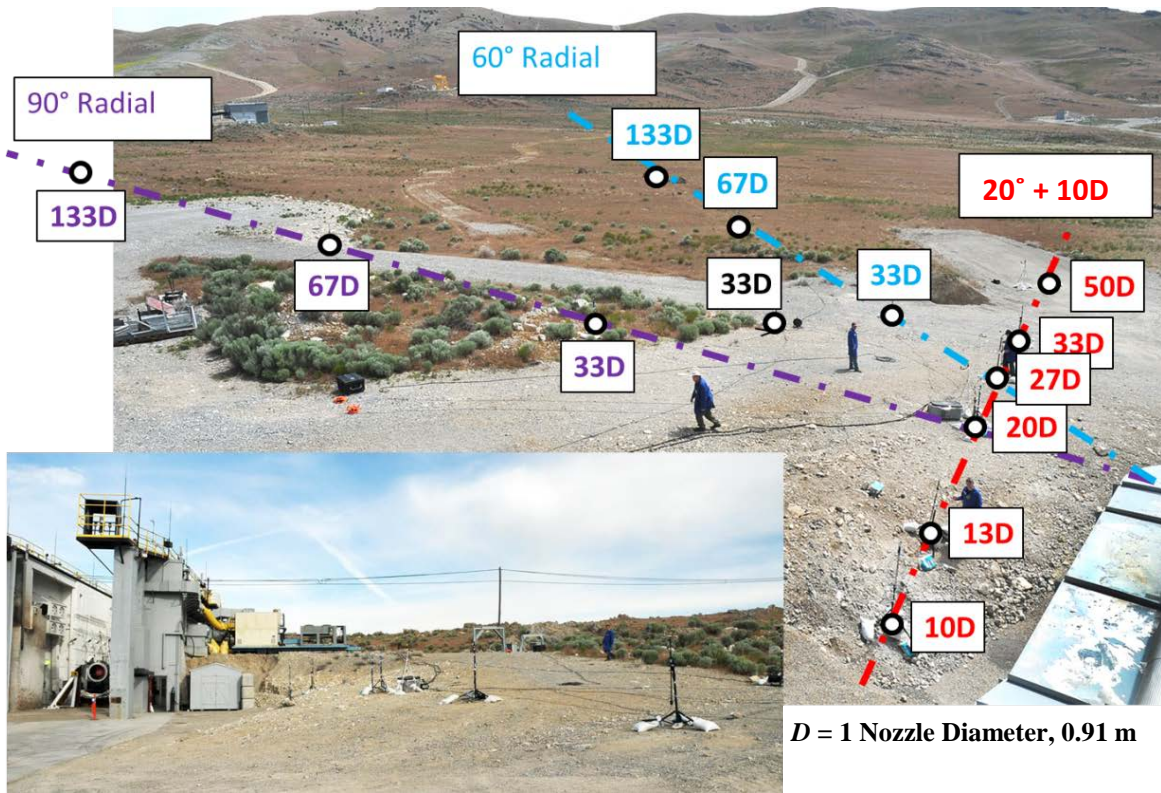


Fig. 3 - Orion-50 measurement layout (red dashed line: shear layer array 20° and 10D offset from rocket centerline with distances relative to nozzle exit; blue and purple dashed lines: 60° and 90° radial arrays, respectively, with distances relative to 15D from the nozzle exit).



Fig. 4 - Orion-50 collocated four-probe measurement layout. Orientation of the four probes and microphones are shown with the plume coming out of the page.

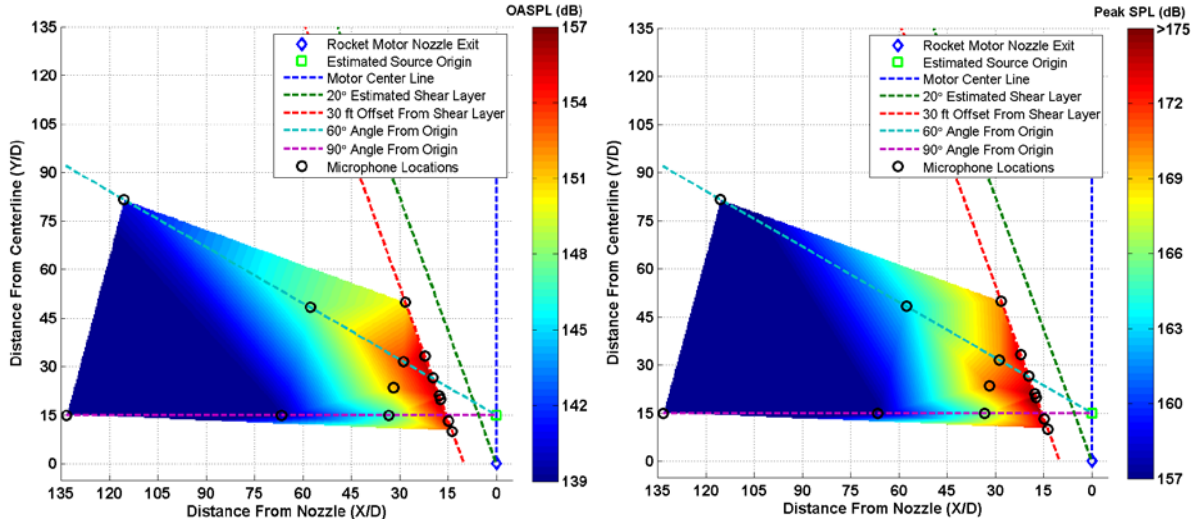


Fig. 5 - Orion-50 spatial pressure maps (left: overall sound pressure level, right: peak sound pressure level).

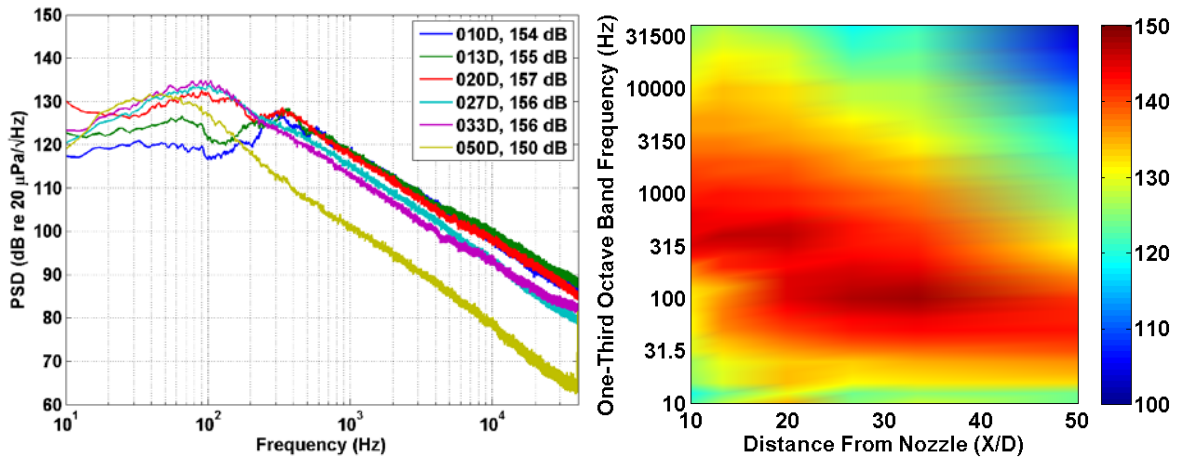


Fig. 6 – Orion-50 measurement shear layer (left: power spectral density, right: one-third octave sound pressure level map).

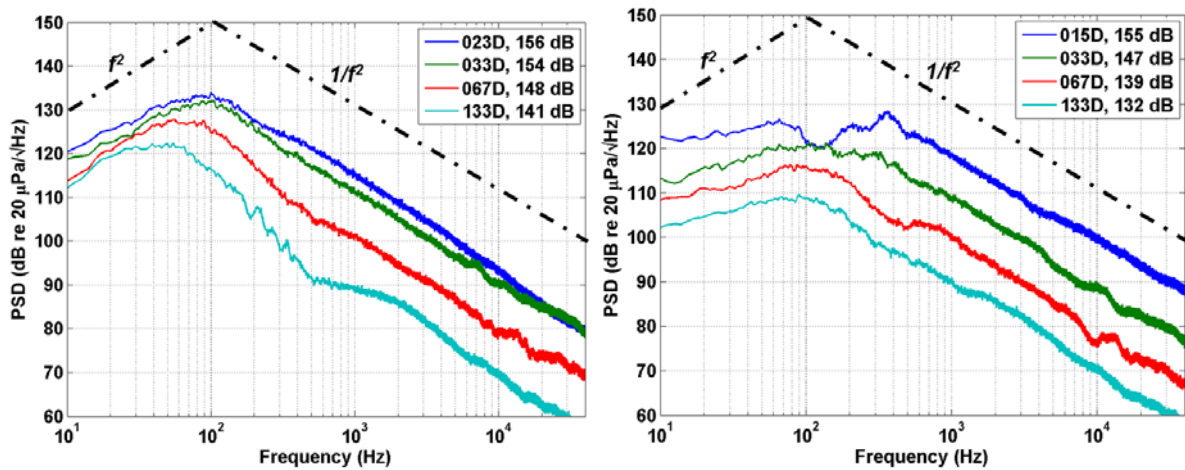


Fig. 7 – Power spectral density computed from microphones along the Orion-50 (left: 60° radial array, right: 90° radial array).

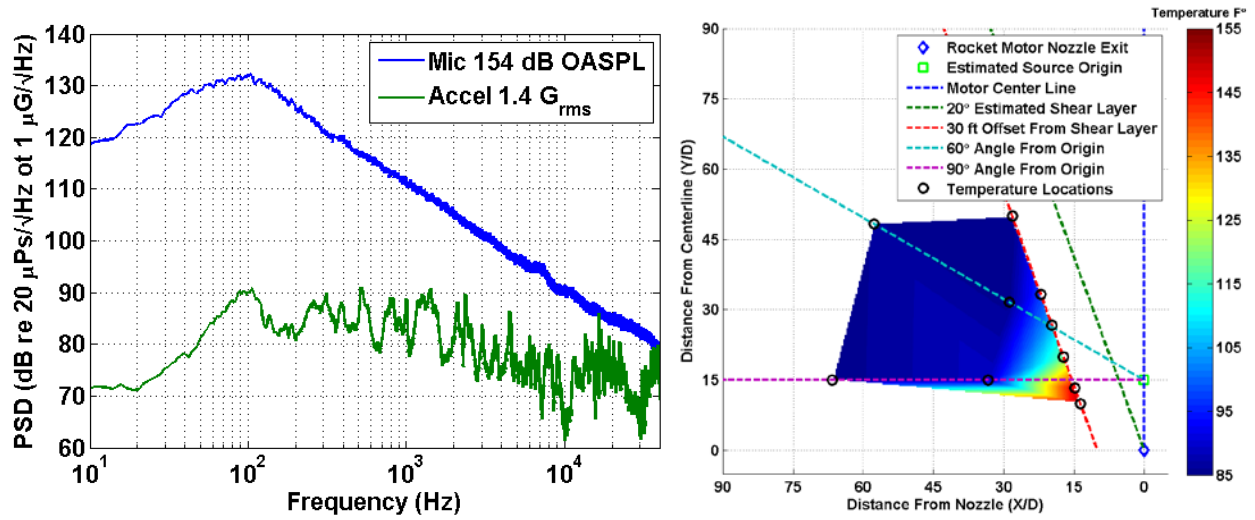


Fig. 8 – Pressure, acceleration, and temperature results. Left: Power spectral density comparison of collocated pressure and vibration sensors located at a distance of 33D on the 60° radial; right: spatial temperature map.

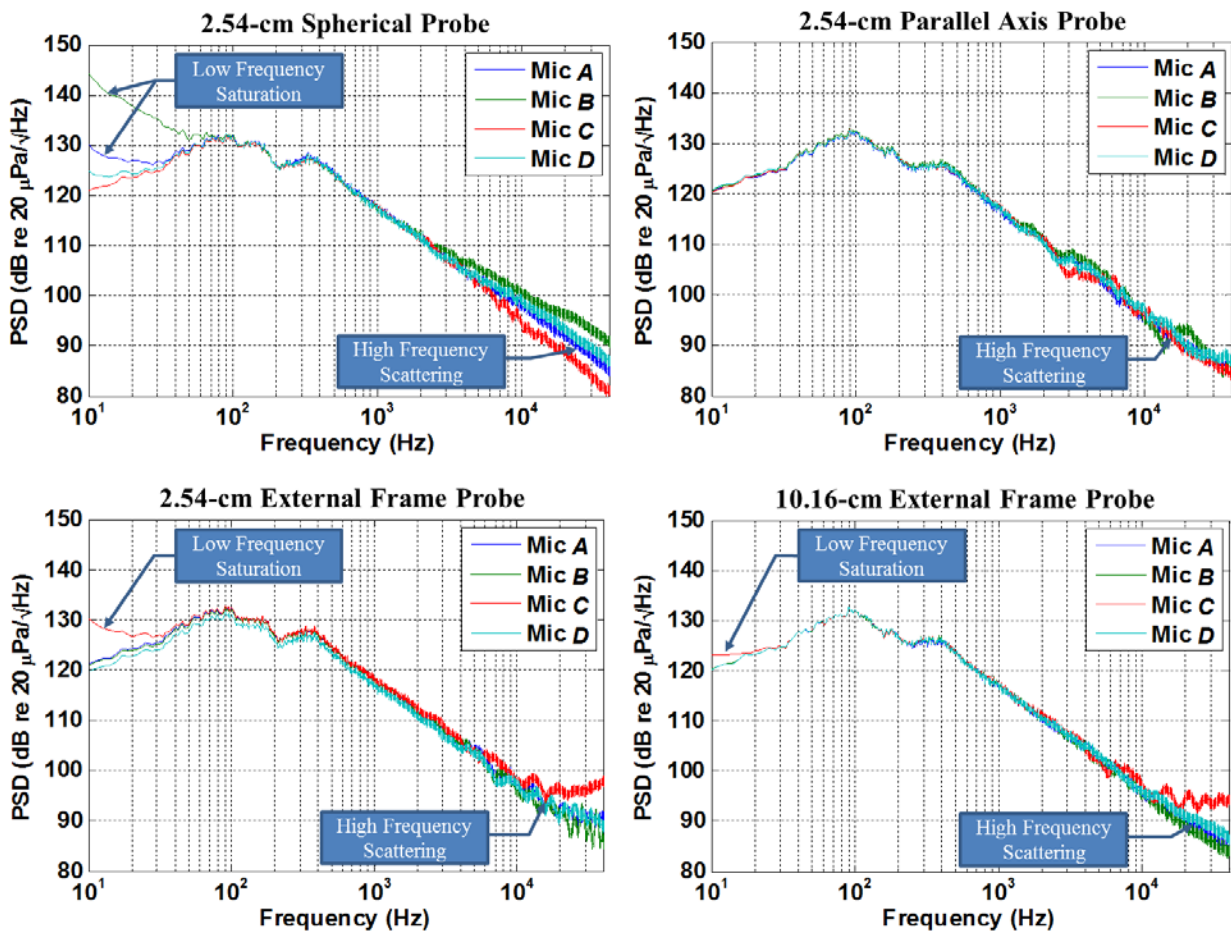


Fig. 9 – Orion-50 power spectral density computed from measurements made with each of the four collocated probe designs.

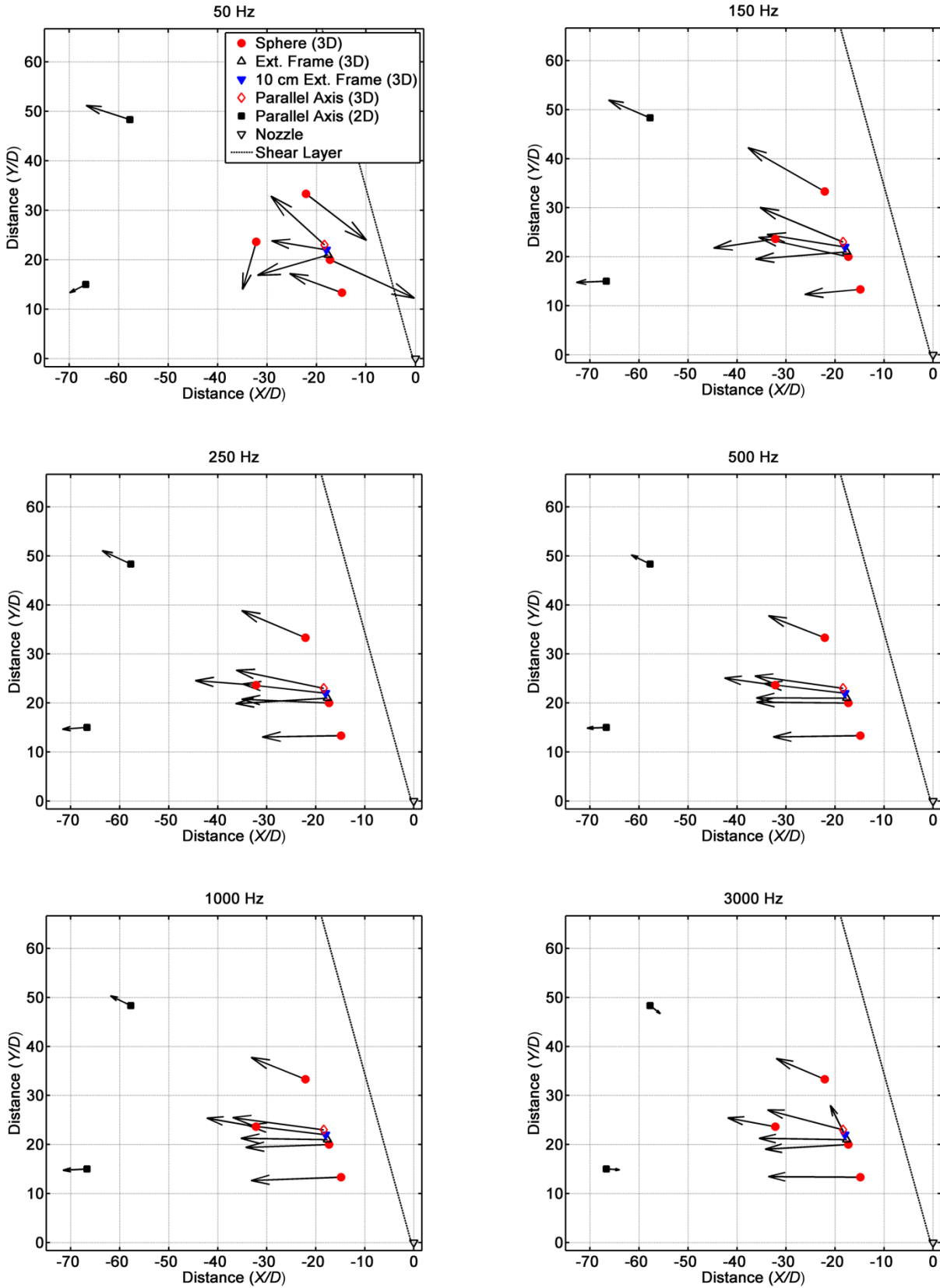


Fig. 10 – Near-field spatial acoustic intensity maps based on Orion-50 probe measurements for various frequencies between 50 and 3000 Hz.